ELSEVIER

Cryogenics 39 (1999) 595–608

Cryogenics

Heat slug propagation in QUELL. Part II: 2-fluid MITHRANDIR analysis

R. Zanino [a,*], C. Marinucci [b,1]

[a] *Dipartimento di Energetica, Politecnico di Torino, 24, c. Duca degli Abruzzi, 10129 Torino, Italy*
[b] *EPFL, CRPP – Fusion Technology Div., CH-5232 Villigen PSI, Switzerland*

Received 17 March 1999; accepted 1 June 1999

Abstract

In this Paper, heat slug propagation in the QUench Experiment on Long Length (QUELL) is studied with the 2-fluid MITHRANDIR model, which allows a finite coupling time between bundle and hole helium in a two-channel cable-in-conduit conductor. The same eight inductively heated and four resistively heated runs are considered in Part I. Good to very good agreement is shown between computed and experimental evolution of the conduit temperature T_{jk} at downstream sensors, as opposed to the poor accuracy of the 1-fluid simulations shown in Part I. The inlet mass flow is typically slightly overestimated, as with the 1-fluid model, resulting in a phase shift between computed and experimental T_{jk}. Some parametric effects are also analyzed.

Keywords: Cable in conduit conductors (A); Superconducting cables (A); Supercritical helium (B); Heat transfer (C); Fusion magnets (F)

Nomenclature

AIN	insulation cross section (m^2)
B	bundle region
E_{cal}	calibrated energy deposited into conductor (J)
F	perforated fraction of helix
FFCORH	artificial multiplier in the correlation for f_H
f_H	friction factor in hole
G_{in}	inlet mass flow rate (kg/s)
H	hole region
h_{eff}	effective heat transfer coefficient between bundle and hole helium
H_{NOWALL}	artificial multiplier for heat transfer coefficient h_{nw} through perforation
H_{WALL}	artificial multiplier for heat transfer coefficient h_w through helix
p_B	helium pressure in cable bundle region (Pa)
p_H	helium pressure in central channel (hole) (Pa)
t	time (s)
T_B	helium temperature in cable bundle region (K)
T_H	helium temperature in central channel (hole) (K)
T_{jk}	temperature of titanium conduit (jacket) (K)
t_{max}	time when T_{max} is reached (s)
T_{max}	peak temperature of titanium conduit (K)
V_B	helium flow speed in cable bundle region (m/s)
V_H	helium flow speed in central channel (hole) (m/s)
x	coordinate along conductor length (m)
Greek	
ΔG_{in}	difference between experimental and computed inlet mass flow (kg/s)
Δ_{kap}	effective thickness of the Kapton layer in the resistive heater
Δt	numerical time step (s)
Δt (T_{max})	time lag between experimental and computed maximum conduit temperature (s)
ΔT_{max}	difference between experimental and computed peak jacket temperature (K)
τ_Q	nominal heating time (ms)
ω	pulse frequency of inductive heater (Hz)

* Corresponding author. Tel.: +39-011-56-44-4490; fax: +39-011-56-44-4499.
E-mail addresses: zanino@polito.it (R. Zanino), claudio.marinucci@psi.ch. (C. Marinucci)
[1] Tel.: +41-56-310-3288; fax: +41-56-310-3729.

0011-2275/99/$ - see front matter
PII: S0011-2275(99)00075-2

1. Introduction

In Part I of the present paper [1] heat slug propagation in QUELL [2] was analyzed with the 1-fluid GANDALF model, which assumes the same pressure and temperature for the helium in the central cooling channel (hole = H) and in the cable region (bundle = B). The 1-fluid model had been validated against QUELL quench data [3] in the past, and also found useful for stability studies [4,5]. However, it was noticed in Part I [1] that for heat slug propagation the predicted jacket temperatures were significantly different from the experimental ones. Indeed, the assumption made in the 1-fluid model of equal B and H helium temperature relies on perfect, i.e., instantaneous coupling between the two regions. On the contrary, the heat slug experiments in QUELL are characterized by relatively low helium flow speeds, O(0.1) m/s in the B region and O(1) m/s in the H region. These give small steady state heat transfer coefficients because the Reynolds number is relatively low, and therefore the B/H coupling is relatively weak.

On the other hand, a 2-fluid model as implemented in the MITHRANDIR code [6], allowing different thermodynamic state of the helium in the B and H regions, can in principle reproduce a finite B/H coupling time as seen in QUELL [7]. This constitutes the main basis for the present analysis.

The same set of 12 heat slug propagation runs (8 inductively and 4 resistively heated), considered in Part I [1], will be studied here using MITHRANDIR. The computed evolution of jacket temperatures at selected sensor locations, together with the evolution of the inlet mass flow, will be compared in detail with the experiment for reference values of the input parameters. The calibration of the resistive heater model already used in Part I will be discussed. A study of the parametric effects of H friction factor, B/H coupling, varying insulation cross section, will be presented, together with a limited study of the numerical convergence of the code. Finally, a few comments on the perspective relevance of the present work for the test programs of the Toroidal Field Model Coil (TFMC) and of the Central Solenoid Model Coil (CSMC), of the International Thermonuclear Experimental Reactor (ITER), will be given.

2. Method

Here we briefly review the major ingredients of the computational method used for the present analysis: 2-fluid model for the helium, choice of B/H coupling and numerical input parameters, resistive heater model.

2.1. Brief overview of the 2-fluid MITHRANDIR model

Previous efforts of 2-fluid modeling of the dual-channel CICC were mostly *analytical*. The simplified case of convection of two different temperature profiles in the two background (given) incompressible flows, exchanging energy by heat conduction, was considered [8,9]. More recently, a diffusion equation was derived [10] for the two temperatures, in the flavor of Taylor–Aris dispersion [11], under the assumption of relatively small temperature difference between B and H, and of same pressure in the two regions. In this model, the temperature diffusion along the conductor arises because of the combined effects of transverse heat conduction and of shear flow in the two regions.

MITHRANDIR solves *numerically* a set of eight partial differential equations in a single spatial coordinate x along the conductor, and time [6]. The unknowns are the pressure, temperature and flow speed along the conductor of B and H helium (p_B, T_B, V_B, p_H, T_H, V_H), and the temperature of strands and jacket (T_{st}, T_{jk}). With respect to the above mentioned analytical efforts, the present model is therefore far more complete in the sense that the compressible transient flow of the helium in the B and in the H region is treated by two separate sets of Euler-like equations. These are coupled by exchanges of mass, momentum and energy (both conduction and convection). Heat conduction in the conduit/jacket and in the strands is also separately treated, coupled by exchanges of energy between solids (through direct contacts) and/or between solid and fluid. Thermodynamic and material properties are obtained from interpolation of tabulated values [16].

2.2. Definition of B/H coupling and numerical input parameters

Geometrical parameters and material constants have already been defined in Part I of the present work [1]. Concerning this subset of the input we shall only elaborate in Section 3 on the effects of different variations of the insulation cross section AIN along the conductor.

In a two-channel topology like QUELL, a heat slug propagates depending strongly on the thermal-hydraulic coupling between the two regions, which is controlled in the 2-fluid MITHRANDIR model by a set of B/H coupling parameters [6]. These include the effective perforated fraction F of the helix, and artificial multipliers (H_{WALL} and H_{NOWALL}) for heat transfer coefficients (see below). In a previous study on QUELL [12], a single *quench* run was used to calibrate these parameters, which were then kept fixed for all other quench runs

studied. [2] The reference B/H coupling parameters, which we use here, are the same determined in that study: $F=0.01$, $H_{\mathrm{WALL}}=1$ and $H_{\mathrm{NOWALL}}=10$, momentum transfer multipliers $\kappa=1$ and $\lambda_v=1$, see Ref. [6] for details. Notice that using the same parameters for both quench and heat slug propagation is not entirely trivial, e.g., other simplified 2-fluid models [10] require different parameters for different type of transients.

Excluding the degenerate case $F=0$, where the pressures in B and H are hydraulically decoupled, it turns out from previous experience with the code that the most important B/H coupling quantity to be considered parametrically is the effective heat transfer coefficient [13], which is given by

$$h_{\mathrm{eff}} = (1-F)\ H_{\mathrm{WALL}}\ h_{\mathrm{W}} + F\ H_{\mathrm{NOWALL}}\ h_{\mathrm{nw}}, \qquad (1)$$

where h_{w} and h_{nw} are the heat transfer coefficients through the helix (standard series of thermal resistances) and through the perforation (derived from Long's model [6]), respectively. Typically, $h_{\mathrm{eff}} \sim 2$–$3\ h_{\mathrm{w}} \sim 500$–$1000$ W/m^2 K.

Because of the uncertainties related to B/H coupling, it is important to perform sensitivity analyses to the values of B/H coupling parameters. Therefore, in Section 3 we shall consider the effects of a reduction of B/H coupling, with respect to the reference case, as enforced by using $H_{\mathrm{NOWALL}}=1$. Notice that a demonstration of the effects of an increase of B/H coupling, with respect to the reference case, is already given by the results of GANDALF [1], which can be considered equivalent to $F\rightarrow 1$, $H_{\mathrm{NOWALL}}\rightarrow\infty$.

Finally, the choice of numerical parameters – the third class of parameters to be defined in the input file – comes directly from a limited convergence study of the code, which is discussed in Appendix A.

2.3. Calibration of the resistive heater model

The resistive heater in QUELL was mounted directly on the Ti conduit and has a rather complex structure [14]. First (i.e., in contact with the conduit) come "two layers of half lap Kapton tapes (0.05 mm)", then "one layer of half lap EGT glass tape (0.13 mm)", then the conducting element comes, a Mn steel wire, 12.2 m long and 0.9 mm in diameter, insulated with 0.03 mm PVF.

In performing preliminary numerical simulations of the resistive runs it turned out that, as already experienced in a previous quench study [12], if the power is input directly to the conduit, then T_{jk} grows much faster and to much higher values than in the experiment, and the simulation becomes meaningless. It is therefore necessary to use some form of heater model at least to approximately describe the delay with which the heat reaches the conduit.

The simple resistive heater model (due to Bottura), which we already used for the quench studies, solves a 1D (radial) time dependent heat conduction equation in a multi-layer medium, *assuming an axially uniform heat source*. However, the heater data above, together with the conduit geometry as given in Part I, Table 3, imply that the heater wire was wound with a very long pitch. Indeed, it occupies in an axial cross-section only $\sim$7% of the available space, i.e., the heat source is actually non-uniform in the axial direction.

In order to find a compromise between resistive heater model and reality, we decided to stick to our 1D model and to artificially increase the thickness of the Kapton. This was done until we were able to approximately reproduce, for the reference values of input parameters, the peak value and the time location of the temperature at the TA3 sensor for run 012. The result of this calibration is shown in Fig. 1, indicating an optimized Kapton thickness $\Delta_{\mathrm{kap}}=2.2$ mm. The same Δ_{kap} was then used for all resistive run simulations. The 1–2 s delay of the TA sensors [1] is not taken into account here, considering that the typical time scale to reach T_{max} is significantly longer. Indeed, it can be observed that the initial computed and experimental evolutions are rather different. Notice finally that in Fig. 1 the different behavior of computed and experimental temperature *after* the peak is mainly due to differences in the background flows (see Section 3).

The same procedure was performed for the GANDALF code as seen in Part I [1], leading in that case to an optimized Kapton thickness of 2.1 mm, i.e., slightly smaller than the value found with MITHRANDIR. This little difference is due to the different B/H coupling assumed in the two models. In the 1-fluid model all the helium is instantaneously available for cooling the jacket. Therefore, *for given input energy and given evolution of* T_{jk}, the needed Kapton layer is thinner than in the case of the 2-fluid model, where the finite B/H coupling time allows only the bundle helium to be instantaneously available.

3. Results and discussion

In this Section we shall present and discuss the results obtained in the simulation with MITHRANDIR of the eight inductively heated runs and of the four resistively heated runs, whose features are summarized in Table 2 of Part I [1]. Each run has been followed for 60 s after the heater was switched on.

[2] Notice that, any time a new conductor is considered with MITHRANDIR, some form of calibration based on available experimental results is useful to determine accurate values of the B/H coupling parameters, since we are at present unable to connect these to the geometrical or technical parameters used in CICC. In the absence of experimental data, a sensitivity study becomes mandatory.

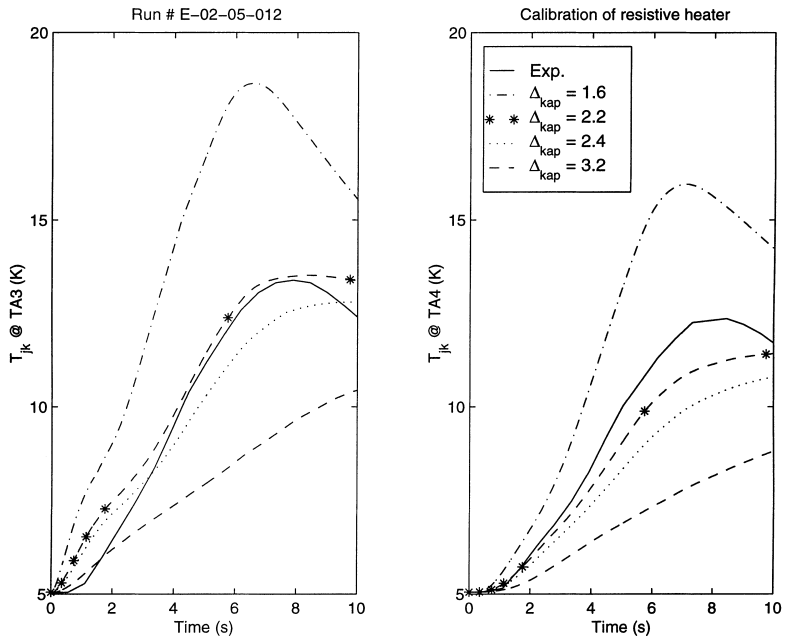

Fig. 1. Validation of the resistive heater model based on the time evolution of the jacket temperature at the TA3 sensor (left plot) during run 012, computed by MITHRANDIR for different Kapton thickness Δ_{kap} in the heater (evolution at TA4 shown for comparison on the right plot). $\Delta_{kap} = 1.6$ mm (dash–dotted), 2.2 mm (symbols), 2.4 mm (dotted), 3.2 mm (dashed). Experiment (solid).

The case of reference input parameters will be considered first, in some detail. For a few selected runs, we shall then address with the 2-fluid model the parametric effects related to: hole friction factor (f_H), bundle/hole coupling (h_{eff}), and variation of insulation cross section (AIN) along the conductor.

4. MITHRANDIR results for reference values of the input parameters

For each experimental run we report the time evolution of the jacket temperature T_{jk} at the sensors TA3–TA8, among which TA5–TA8 are shown on a fixed scale. The spatial profiles of T_{jk} at $t = 10$ s and at $t = 20$ s are also presented, for a clear indication of the diffusion of the heat slug along the conductor. Finally, the time evolution of the total inlet mass flow G_{in} is given.

Let us consider first the case of the inductively heated runs. The results concerning the runs at $\omega = 952$ Hz (i.e., runs 001–004) are presented in Fig. 2, while those at $\omega = 590$ Hz (i.e., runs 005–008) are shown in Fig. 3.

First of all, it can be noticed that there is typically a good agreement, particularly in the peak values, between experimental and MITHRANDIR conduit temperature at the far downstream sensors (TA6–TA8), except for a phase shift in the curves (see below for a further discussion of this point). Concerning the 'heater sensors' (TA3–TA4), however, a typically faster increase and higher peak is observed in the simulations, compared with the experiment. This is not a numerical artifact (see Appendix A), but it is rather likely an effect of the time delay in the sensor signal [1,2], related to how the sensors themselves are mounted on the conduit. At the intermediate sensor TA5 the agreement is good for low input energies E_{cal} (run 001, 005, 006), while it becomes worse for increasing input energy.

Concerning the inlet mass flow, we can observe that a significant perturbation of G_{in} arises in the very first phase of the simulated transient. This can lead to an increasing reduction of G_{in} in the lowest energy runs (005, 001, 006), to a choking of the inlet flow for intermediate energies (run 002), or even to increasingly reversed flow for the highest input energies (run 007, 008, 003, 004). This perturbation arises on the sound time scale, i.e., the time needed for the sound wave originated at the heater to reach the conductor inlet. For a typical sound speed value of ~200 m/s this gives a time scale ~0.2 s, which is however too fast to be detected with the 2 Hz resolution of the experimental diagnostics.

On the longer time scale, the inlet mass flow is more or less constant and slightly overestimated by MITHRANDIR (see below for a discussion of this point). The reason for the oscillations in G_{in} is the same as in GANDALF and was discussed in Part I [1].

Let us now consider the results for the resistively heated runs (009–012) which are reported in Fig. 4.

Here we can see that there is typically a very good agreement between experimental and MITHRANDIR conduit temperature for all runs and at all sensors, with still some phase shift. In particular at the heater sensor TA3 the agreement appears to be good not only on run

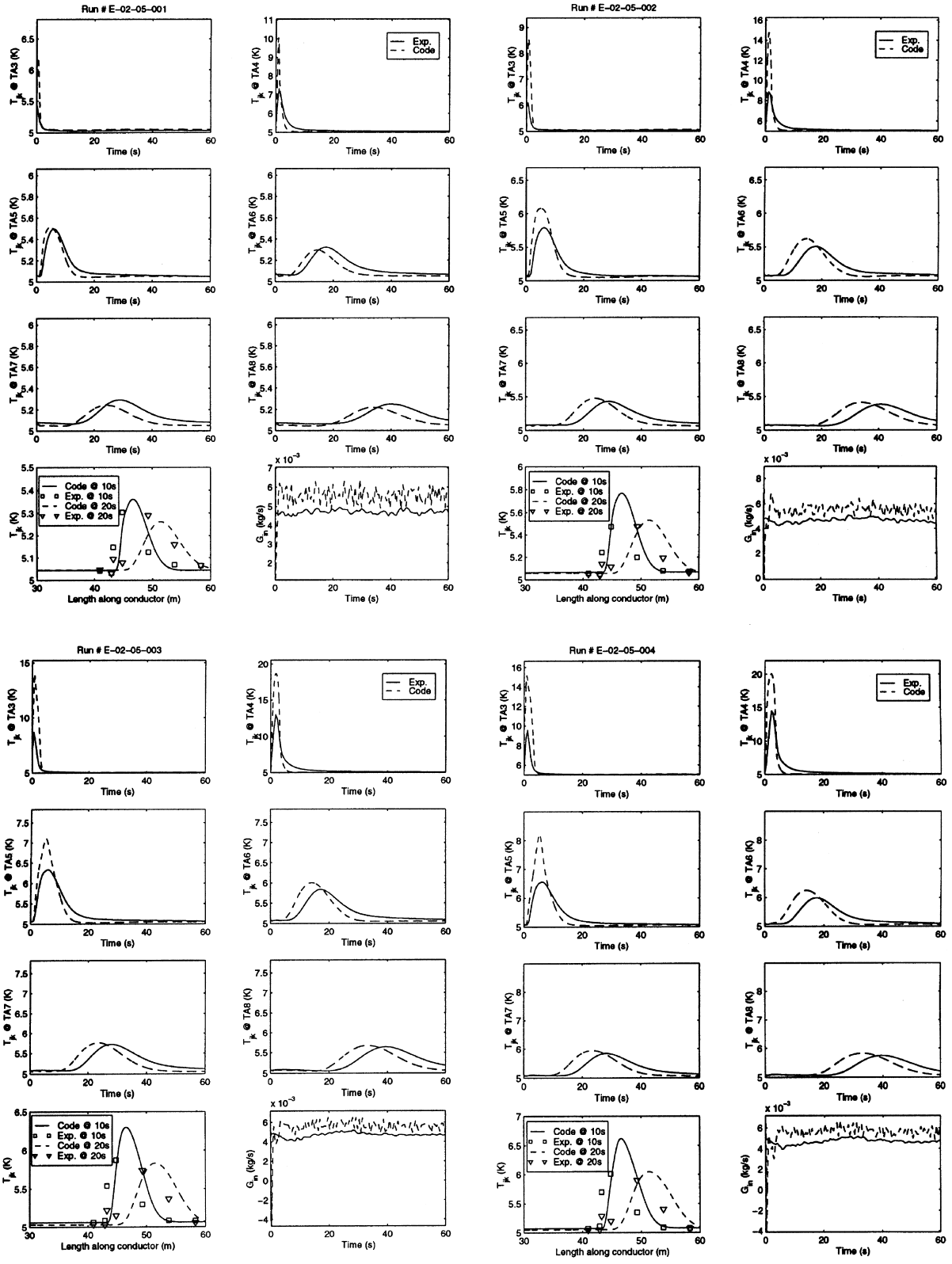

Fig. 2. Summary of results for all inductive runs @ 952 Hz (001 upper left subplot, 002 upper right subplot, 003 lower left subplot, 004 lower right subplot). Comparison between the time evolution of experimental (solid lines) and MITHRANDIR (dashed lines) jacket temperature at sensors TA3-8 (top 6 sub-subplots). Experimental (symbols) and MITHRANDIR (lines) jacket temperature profiles along the conductor @ $t = 10$ s and 20 s (lowest left sub-subplots). Total experimental (solid) and MITHRANDIR (dashed) inlet mass flow (lowest right sub-subplots).

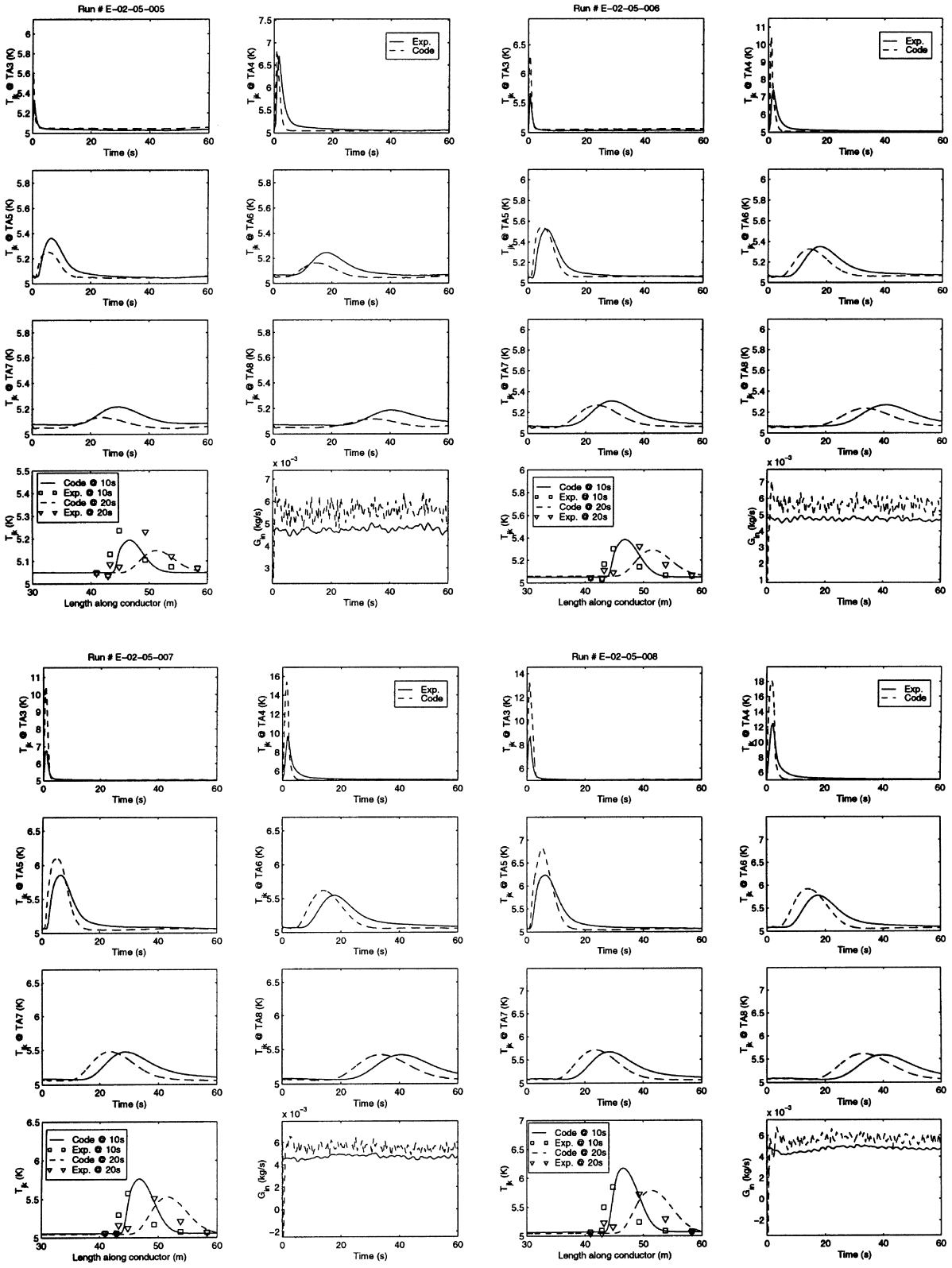

Fig. 3. Summary of results for all inductive runs @ 590 Hz (005 upper-left subplot, 006 upper right subplot, 007 lower left subplot, and 008 lower right subplot). Comparison between the time evolution of experimental (solid lines) and MITHRANDIR (dashed lines) jacket temperature at sensors TA3-8 (top 6 sub-subplots). Experimental (symbols) and MITHRANDIR (lines) jacket temperature profiles along the conductor @ $t = 10$ s and 20 s (lowest left sub-subplots). Total experimental (solid) and MITHRANDIR (dashed) inlet mass flow (lowest right sub-subplots).

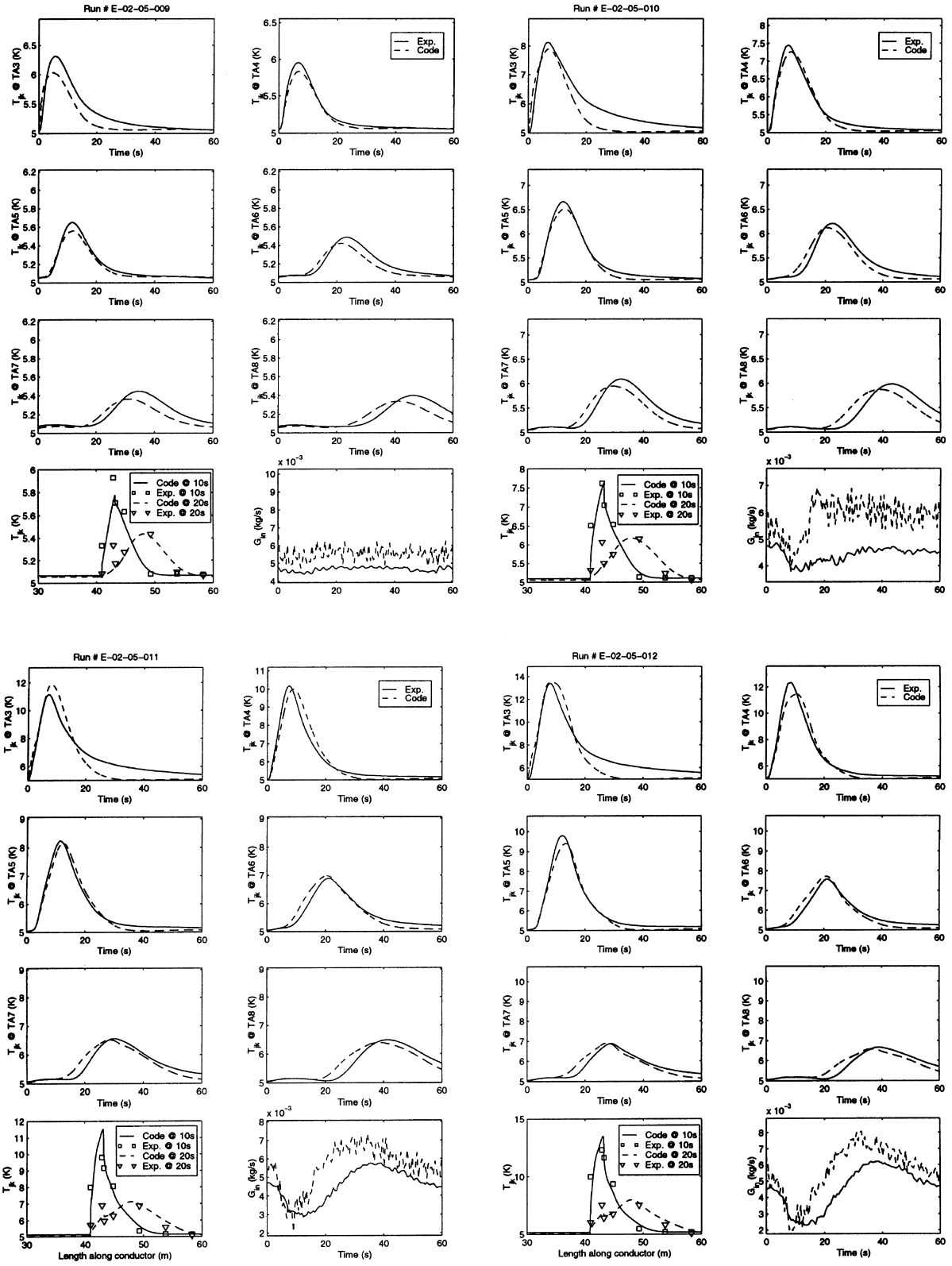

Fig. 4. Summary of results for all resistive runs (009 upper-left subplot, 010 upper right subplot, 011 lower left subplot, and 012 lower right subplot). Comparison between the time evolution of experimental (solid lines) and MITHRANDIR (dashed lines) jacket temperature at sensors TA3-8 (top 6 sub-subplots). Experimental (symbols) and MITHRANDIR (lines) jacket temperature profiles along the conductor @ $t = 10$ s and 20 s (lowest left sub-subplots). Total experimental (solid) and MITHRANDIR (dashed) inlet mass flow (lowest right sub-subplots).

012, on which the heater calibration was based, but also for all other runs. In a different representation, the significantly peaked spatial profiles at $t = 10$ s, and their diffusion at $t = 20$ s are well reproduced by MITHRANDIR.

Concerning the inlet mass flow G_{in}, we notice first of all that at the lowest input energy E_{cal} (run 009) no significant perturbation arises, i.e., the considered transient is a 'true' heat slug, convected downstream by the given incompressible G_{in}. At increasing input energy, however, the perturbation of G_{in} can become significant. The generation of the slug, and its attempt to expand upstream, lead to a slight reduction of G_{in} in the initial phase of the transient for intermediate input energies (run 010), and to more strongly reduced flow at the conductor inlet for further increasing E_{cal} (run 011, 012). In the second part of the transient, the mass flow 'bounces back', and the stronger the higher the input energy was. The associated compressible flow effects are at least qualitatively reproduced by the code. Quantitatively, the inlet mass flow appears again to be slightly overestimated by MITHRANDIR during most of the transient (the apparently larger discrepancy in run 010 is only an effect of the scale used in the plot).

In both inductive and resistive runs we can conceptually split the difference between simulated and experimental T_{jk} in two parts: (1) difference in the peaks T_{max}, (2) phase shift. While the second point will be addressed below, we report in Table 1 a synthetic quantitative comparison between measured and computed T_{max} and total ($B + H$) inlet helium mass flow G_{in}, restricted to the runs analyzed in Part I [1]. *The agreement between experimental and MITHRANDIR T_{max} is for all runs significantly better than what obtained with the 1-fluid GANDALF model* [1]. We notice that the absolute error in the peaks is typically ~0.1–0.2 K, and this is ~2–3 % if normalized to T_{max}. Obviously, if the temperature *jump* were used for normalization, then the relative error would correspondingly increase, particularly for very low energy input. Notice finally that the total inlet mass flow (except for very high-energy input) is typically overestimated by ~20% with MITHRANDIR, i.e., essentially the same as with GANDALF [1]. This similarity is not surprising since the *2-flow* model, describing different helium flow speeds in B and H (as opposed to a *2-fluid* model, assuming different thermodynamic state for the helium in the two regions), is essentially common to both codes.

Table 1
Differences in T_{max}[a] and G_{in}[b] between MITHRANDIR and experiment

Run	$\lvert\Delta T_{max}\rvert$ (K)	$\lvert\Delta T_{max}\rvert/T_{max}$[c] (%)	$(\Delta G_{in}/G_{in})$[d] (%)
005	0.08	1.6	19
008	0.20	3.3	24
009	0.11	2.1	20
012	0.17	2.0	35[e]

[a] Max (T_{jk}) at sensors over whole transient.
[b] Total (B + H) inlet helium mass flow.
[c] Average over downstream sensors TA5–8.
[d] Time average over whole transient.
[e] Average for $0 < t < 15$ s $\rightarrow (\Delta G_{in}/G_{in}) \sim 22\%$.

Table 2
Maximum in time of $\lvert T_B - T_H\rvert$, with sign, computed by MITHRANDIR at different sensors for runs 008 and 012

Sensor	Max for run 008 (K)	Max for run 012 (K)
TA3	+5.9	+3.3
TA4	+10.0	+2.3
TA5	−1.3	−0.92
TA6	−0.32	−0.52
TA7	−0.16	−0.31

In order to provide the physical basis for a comparison with the 1-fluid results of Part I [1], we report in Table 2 the maximum (in time) temperature differences between B and H, *with their sign*, computed with MITHRANDIR at different sensors, for runs 008 and 012. We notice that at the heater sensors (TA3–TA4) the B helium is warmer than the H helium, because of its direct contact with the heated jacket. On the contrary, at the downstream sensors the H helium is warmer than the B helium, although the temperature difference is smaller. This is due to the fact that the helium in the central channel travels downstream significantly faster than the helium in the cable bundle, because of the lower friction, and thus *preheats* the bundle [13]. The finite coupling time between bundle and hole helium, together with the difference in the respective flow velocities, provides the additional diffusion mechanism, peculiar of the 2-fluid model, which is needed to obtain a good agreement with the experiment. Of course these temperature differences between the two regions cannot be present in the 1-fluid model, which sees only *an* average T for both B and H helium. [3] Table 2 provides therefore also a qualitative explanation, as given in the Summary Section of Part I [1], of the disagreement of the 1-fluid results with the experiment.

4.1. Effect of different values of the hole friction factor

It was observed above (and quite similarly in Part I, using the GANDALF code) that the computed mass flow at conductor inlet is typically higher than the experi-

[3] Notice that the helium temperature T foreseen by GANDALF at a given time and location needs *not* be between the T_B and T_H foreseen by MITHRANDIR. Indeed, this is typically the case only below the heater, where a 0-D argument based on the heat capacities of bundle and hole helium applies. Away from the heater the behavior is 1-D. In the 1-fluid model the convection of $T < T_B$ happens with a flow speed $V \sim (V_B A_B + V_H A_H)/(A_B + A_H) > V_B$ [10]. Therefore, at the downstream sensors it can happen that $T > T_B$, T_H, as is the case in, e.g., both run 008 and run 012 (compare Figs. 4 and 6 in Part I [1] with Figs. 2 and 3 and Table 2 here).

mental value. In view of the fact that experimental pressures are used as time dependent boundary conditions, so that these cannot be responsible for the disagreement, we have attributed this discrepancy to the use of a not fully appropriate value for the friction factor. Considering that most of the helium flows in the central channel, and that the Katheder correlation for the friction factor in the bundle (see Part I [1]) should be fairly accurate, the discrepancy could be due mainly to an inaccuracy of the friction factor in the hole, f_{H}. While sticking to the suggested correlation [15] $f_{\mathrm{H}} = \mathrm{FFCORH} \times 0.046/Re^{0.2}$, where Re is the Reynolds number in the hole, we study the effect of a correction factor FFCORH = 3.0, different from the suggested [15] value FFCORH = 2.5, which we used as reference until now. Considering the data on which the correlation is based [15] this variation in FFCORH appears to be still acceptable.

The above mentioned effect is considered in detail in Fig. 5 only for two representative runs: one inductive (008) and one resistive (012). Concerning run 008 we can notice that the reduced mass flow at inlet, caused by stronger friction in the hole, leads to a slower traveling slug and reduces the phase shift with the experiment (the slightly higher peaks can also be attributed to additional heating due to the stronger friction). Concerning run 012 similar features can be noticed. Additionally it has to be mentioned that the calibration of the resistive heater should obviously be repeated in this case, in order to reproduce the optimal agreement at the heater sensors, which we have by definition in the reference case.

The reduction in phase shift between experimental data and MITHRANDIR results, due to increased f_{H}, is more quantitatively reported in Table 3. Here the time lag Δt ($T_{\max}$) between the experimental and computed maximum conduit temperature at the three far downstream sensors TA6–TA8 is given for all runs considered here. We notice that a relatively small variation (FFCORH from 2.5 to 3) can indeed lead to significantly better agreement between code and experiment ($\sim$50% or more reduction in the phase shift).

The effect of the friction factor was not investigated with GANDALF because it is a secondary effect there, compared to the primary temperature discrepancies reported in Part I [1].

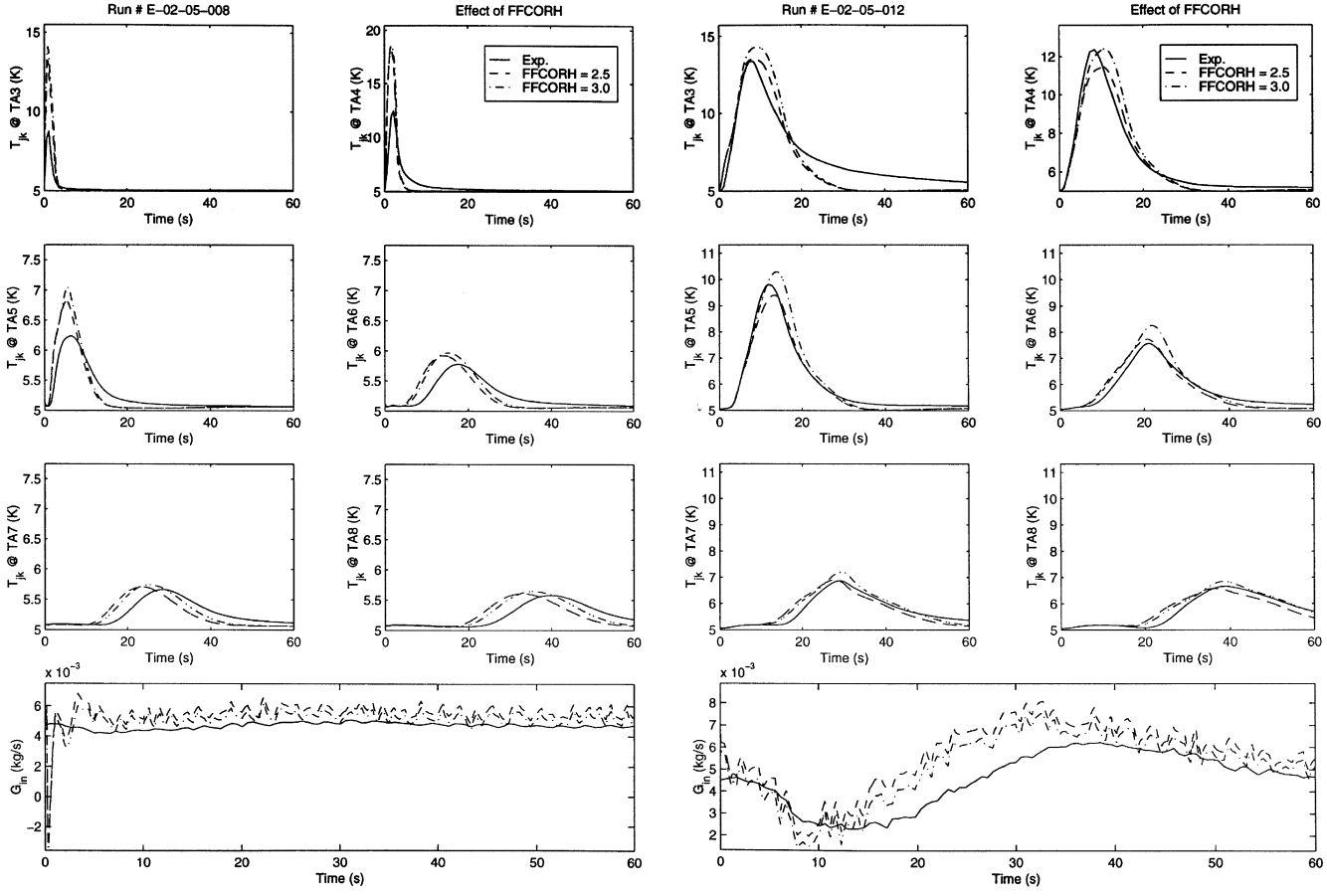

Fig. 5. Effect of different values of the correction factor FFCORH for the hole friction factor f_H. Results of inductive run 008 (left subplot) and of resistive run 012 (right subplot). Experiment (solid lines), MITHRANDIR with reference FFCORH = 2.5 (dashed lines), MITHRANDIR with FFCORH = 3.0 (dash–dotted lines). Jacket temperature at sensors TA3-8 (top 6 sub-subplots), total inlet mass flow (lowest sub-subplots).

Table 3
Effect of FFCORH[a] on $\Delta t(T_{max}) \equiv t_{EXP}(T_{max}) - t_{CODE}(T_{max})$ at sensors[b]

Run #	$\Delta t(T_{max})$ @ TA6 (s)	$\Delta t(T_{max})$ @ TA7 (s)	$\Delta t(T_{max})$ @ TA8 (s)
001	3.0	4.6	6.9
	2.1	**2.5**	**3.6**
002	3.5	5.1	6.6
	2.2	**3.0**	**4.1**
003	2.8	4.6	6.1
	1.9	**3.0**	**3.7**
004	3.0	4.0	6.3
	1.7	**2.8**	**4.2**
005	4.0	6.3	4.9
	1.6	**5.3**	**3.2**
006	3.8	4.7	6.5
	2.1	**3.5**	**4.9**
007	4.1	5.5	7.7
	2.8	**3.2**	**4.3**
008	3.5	5.5	6.9
	2.2	**3.2**	**4.6**
009	2.0	3.3	4.9
	1.5	**1.9**	**1.9**
010	1.3	2.6	4.8
	0.5	**0.8**	**2.4**
011	0.6	1.9	2.5
	−0.6	**−0.1**	**0.5**
012	0.2	1.3	2.9
	−0.9	**−0.6**	**0.6**

[a] Correction factor for friction factor correlation in hole.
[b] FFCORH = 2.5 → normal values, FFCORH = 3.0 → boldface values.

5. Effect of reduced *B*/*H* coupling

Modeling of the B/H coupling in a dual channel CICC is very difficult because of the complex geometry of the interface and of the resulting flow pattern. The typically turbulent flow, with Reynolds numbers $\sim 1\text{–}2 \times 10^5$ in the central channel for the cases considered here, and the related heat transfer can indeed be significantly influenced by several parameters. These include the radial thickness, pitch, and axial width of the helix, and its *effective* perforated fraction (i.e., what is not occluded by the strands on the B-side of the nominal perforation). Our present ignorance in this matter forces us to use (see above) artificial multipliers in the formulation of the B/H coupling model. In view of these difficulties we have performed for the same two representative runs as above (i.e., run 008 and 012) a limited study of the effects related to a reduction of B/H coupling. This reduction was enforced by using an artificial multiplier $H_{NOWALL} = 1$ for the heat transfer coefficient h_{nw} through the perforation, instead of the reference value $H_{NOWALL} = 10$. For a full appreciation of the results below, notice however that this does not amount to a tenfold reduction of the heat flux through the perforation, because some form of self-regulating mechanism in the model leads simultaneously to a larger temperature difference between B and H [13].

The results of this study are reported in Fig. 6. We notice that the qualitative response to a reduction of B/H coupling is not different between inductively and resistively heated run. While the inlet mass flow is not dramatically influenced by a reduction of B/H coupling, the conduit temperature is more markedly affected, and in qualitatively different ways depending on the position along the conductor. In particular, near the heater we observe a higher peak of the computed T_{jk} for lower H_{NOWALL}, whereas at the downstream sensors the situation reverses, showing lower and broader (in time) T_{jk} for lower H_{NOWALL}. This behavior can be easily explained by considering Table 2 again. In proximity of the heater a lower B/H coupling implies warmer helium in the bundle, and therefore a higher T_{jk}. On the contrary, far downstream from the heater a lower B/H coupling implies (see Part I [1]) a stronger diffusion of the helium temperature profile, i.e., T_B, and therefore T_{jk}, are broader and lower.

6. Effect of different variations of the insulation cross section AIN along the conductor

In all previous QUELL studies performed with GANDALF and/or MITHRANDIR, the insulation was assumed to be present *all along the conductor*. In the preparation of the present study we realized that it was actually present only outside the resistive heater region. As seen in Part I [1] we decided therefore to use for the present study AIN = 0 as reference input parameter, all along the conductor. However, a version of MITHRANDIR has been developed which is now able to deal with (discontinuous) variations of AIN along the conductor. (This was done particularly in view of future applications to the TFMC and CSMC test program analysis, where the *simultaneous* simulation of conductor and joints will require this kind of capability from the codes). In this Section we shall therefore consider three different cases: (1) AIN = 0 everywhere (reference); (2) AIN = 344.14 mm^2 everywhere (actual *approximate* cross section area in the non-heated region); (3) AIN = 344.14 mm^2 for $x < 40.5$ m, and for $x > 43.5$ m, while AIN = 0 for 40.5 m $< x <$ 43.5 m.

The results of this study are shown in Fig. 7 for the same two representative runs as above (i.e., run 008 and 012), limited to cases 1 and 2. Case 3 gives essentially the same results as case 1, because of the dominating helium heat capacity, and is not shown for clarity.

We notice first of all that the inlet mass flow is not dramatically affected by the value of AIN. On the other hand, the conduit temperature, and in particular the peaks at the heater sensors where the time profiles are narrower, decrease if the insulation is taken into account, because part of the energy input goes into the heat capacity of the insulation.

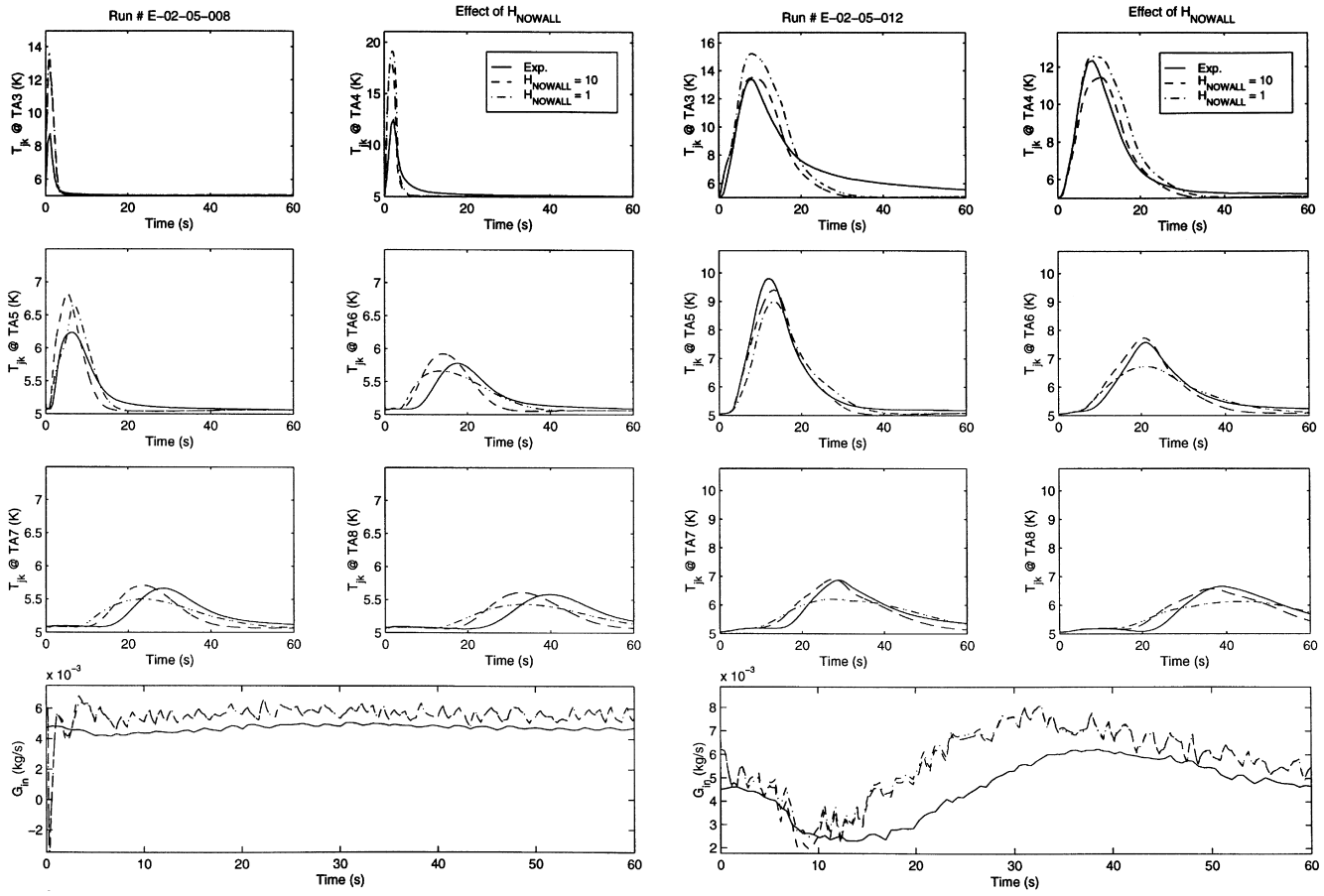

Fig. 6. Effect of different values of the correction factor H_{NOWALL} for the B/H heat transfer coefficient h_{nw} through the perforation. Results of inductive run 008 (left subplot) and of resistive run 012 (right subplot). Experiment (solid lines), MITHRANDIR with reference $H_{\mathrm{NOWALL}} = 10$ (dashed lines), MITHRANDIR with $H_{\mathrm{NOWALL}} = 1$ (dash–dotted lines). Jacket temperature at sensors TA3-8 (top 6 sub–subplots), total inlet mass flow (lowest sub-subplots).

As a final remark it can be noticed that, if one is interested in improving the accuracy, the heater calibration should be repeated, any time a different value/variation for AIN is considered. Here this was not done, since a study of the parametric effects of AIN obviously requires keeping all other parameters fixed.

7. Conclusions and perspective

The MITHRANDIR code has been successfully validated against a set of twelve heat slug propagation runs in QUELL, with heater lengths from 0.12 m (inductive) to 2.3 m (resistive), nominal heating duration from 40 ms (inductive) to 300 ms (resistive), and calibrated input energies from ~40 J to ~1600 J.

Notwithstanding the broad range of parameter variation, the 2-fluid model implemented in the MITHRANDIR code has proved to be able to accurately simulate the evolution of the jacket temperature at different sensor locations, as opposed to a 1-fluid model [1]. The total helium mass flow was typically overestimated by ~20%, as with the 1-fluid model, most likely because of an inaccurate correlation for the friction factor in the hole.

Finally, a number of parametric effects has been considered and elucidated.

In the perspective, some comments on TFMC and CSMC relevance of the present work may be relevant. It was already mentioned in the Introduction to Part I [1] that the present work finds part of its justifications in the renewed interest on heat slug propagation, recently arisen in the framework of the ITER Model Coils [17–20] test program. Let us now briefly consider the relations between that program and this work.

We can observe first of all that the accuracy of the 2-fluid results is certainly encouraging. Furthermore, if compared with the TFMC and CSMC 'true' heat slugs, we have seen above that the QUELL transients considered here can sometimes significantly influence the background flow, and as such they can be considered harder to reproduce numerically than a true heat slug traveling in a fixed background flow. Finally, as already pointed out, the variable AIN extension of

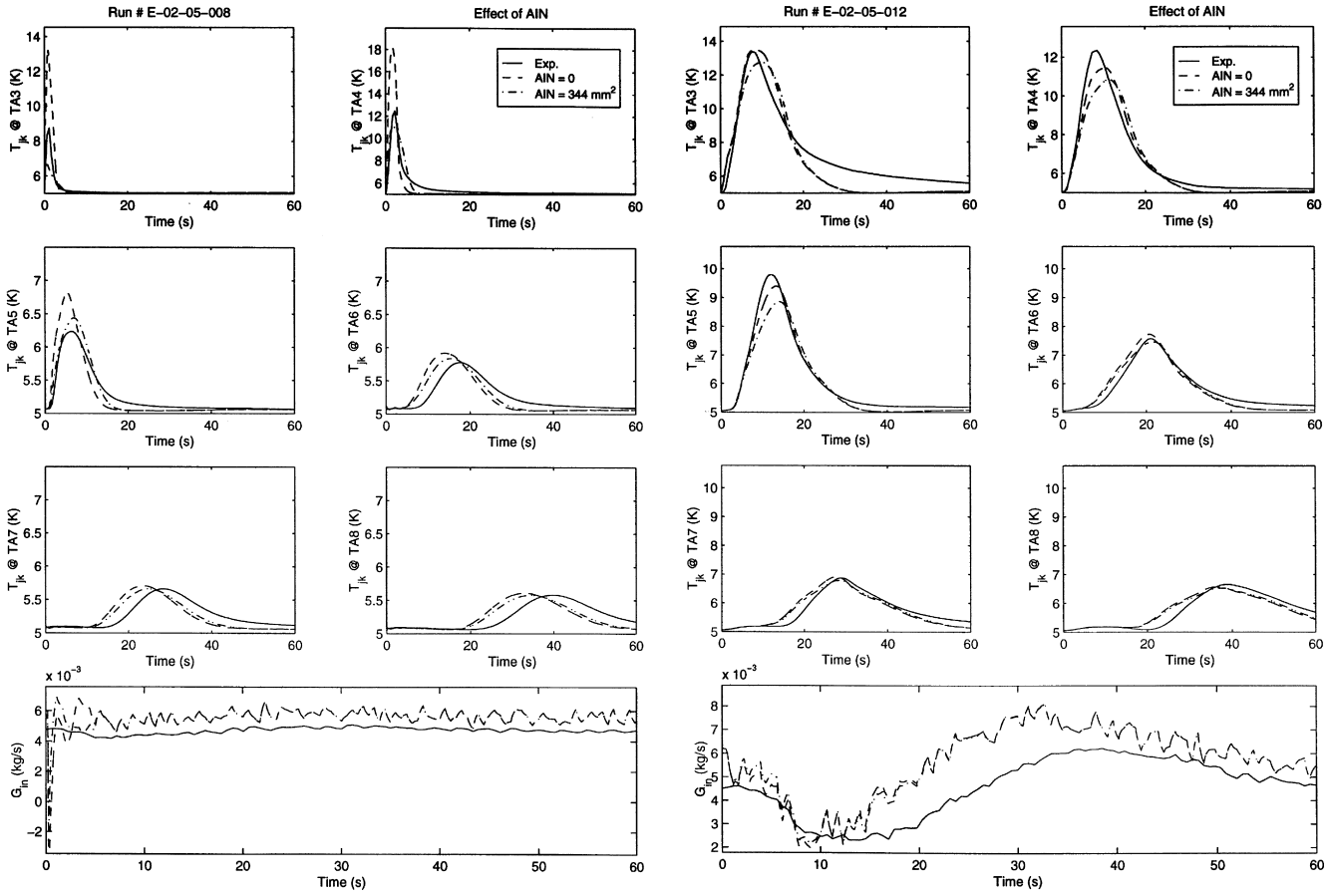

Fig. 7. Effect of different values of the insulation cross-section AIN, *assumed to be uniform along the conductor*. Results of inductive run 008 (left subplot) and of resistive run 012 (right subplot). Experiment (solid lines), MITHRANDIR with reference AIN = 0 (dashed lines), MITHRANDIR with AIN = 344 mm^2 (dash–dotted lines). Jacket temperature at sensors TA3-8 (top 6 sub–subplots), total inlet mass flow (lowest sub-subplots). Results (not shown) obtained by MITHRANDIR with a more accurate, variable AIN(x) along the conductor (see text) essentially coincide with those of the reference case.

MITHRANDIR can open the way to a possible common treatment of joint and conductor, which will be an essential ingredient of the Model Coil analysis.

On the open problems side, we can observe first of all that in the Model Coils the heater will be located upstream of the conductor, i.e., the heat slug model will require a sufficiently accurate treatment of the external hydraulic circuit [21]. Secondly, the heat slug shall be used to (possibly) initiate a quench, and the simulation of this multiple space and time scales transient has never been attempted yet with MITHRANDIR. Finally, some CSMC specific problems will arise related, e.g., to the fact that several thermally coupled parallel hydraulic paths of the two-in-hand conductor will need to be somehow taken into account in the simulation.

Acknowledgements

The European Community Fusion Technology Program under contracts to R.Z. and C.M. has partially financially supported this work. We also wish to thank L. Bottura (CERN) and L. Savoldi (POLITO) for discussions on the subject of this paper. A preliminary version of this report was presented at the 2nd TFMC Test Group Meeting at Forschungszentrum Karlsruhe, Germany, on February 4 1999, and comments from several participants to the meeting are also gratefully acknowledged. Finally, we are thankful to one referee for several observations, which led to an improvement of the readability of the paper.

Appendix A. Numerical stategy, convergence and computational performance of the MITHRANDIR code applied to heat slugs

Here we wish to briefly discuss the numerical strategy employed for the present heat slug study, and show convergence in the sense of *approximate independence of the solution from mesh and time step*. This is essential in order to guarantee that features of the numerical solu-

Table 4
Results of numerical convergence study on run 008

Case	NELEMS	NELREF	STPMIN (s)	STPMAX (s)	STPMAX2 (s)	T_{max} (K) @ TA3	t_{max} (s)	T_{max} (K) @ TA4	t_{max} (s)	T_{max} (K) @ TA5	t_{max} (s)
A	1354	80	**1e−5**	**1e−3**	**5e−2**	14.9	0.85	18.9	1.7	7.1	5.3
B	1434	160		–	–	13.8	0.85	18.4	1.6	6.9	5.2
C	**1594**	**320**	–	–	–	13.2	0.85	18.1	1.6	6.8	5.3
D	1914	640	–	–	–	12.9	0.85	18.0	1.6	6.8	5.3
E	2896	320	–	–	–	13.2	0.84	18.1	1.6	6.7	5.4
F	1594	320	–	5e−4	–	13.3	0.85	18.2	1.6	6.8	5.3
G	–	–	–	1e−3	1e−2	13.2	0.84	18.1	1.6	6.8	5.3
H	–	–	–	–	5e−3	13.3	0.84	18.1	1.6	6.8	5.3
J	–	–	1e−6	–	5e−2	13.3	0.84	18.2	1.6	6.8	5.2

tion do not significantly depend on the discretization, and to determine the minimal (i.e., computationally least expensive) set of *numerical parameters* giving a reliable solution, see Table 4 below.

Space discretization is done with Galerkin linear finite elements for all terms except the convective ones, which are treated by a stabilizing upwind formulation. A fixed mesh with NELEMS total elements is used, refined around the heater from $x = \text{XBREFI}$ to $x = \text{XEREFI}$ in order to properly resolve in space the heated region (NELREF elements are located in this region). In each sub-domain the mesh is uniform.

Time discretization is done with finite differences, using the backward Euler (fully implicit) scheme. In order to properly resolve the heated phase in time, we distinguish between two periods in the transient. From $t = 0$ (pulse start) to $t = 5 \times \tau_Q$ the time step Δt is increased automatically from STPMIN to STPMAX. For $t > 5 \times \tau_Q$ the maximum time step allowed is increased to STPMAX2 > STPMAX.

Convergence of the MITHRANDIR code in the strict sense, i.e., reduction of the numerical error with a certain power of mesh and time step, was already demonstrated in the past [6], for a model quench study. Here we restrict our considerations to inductive runs, which are more critical because of the extreme localization of the source both in space (0.12 m) compared with the extension of the domain (∼91 m), and in time (40 ms) compared with the typical duration of the transient (60s). We further limit our study to the case of run 008 only. As a measure of the mesh independence of the full numerical solution, we arbitrarily decided to concentrate only on the maximum value T_{max} of T_{jk} reached at the sensors TA3, TA4 and TA5 and on the instant t_{max} when this maximum is reached. (Those sensors were picked considering the disagreement between computation and experiment shown at their locations, see Section 3). The mesh is refined in all cases between XBREFI = 42.72 m and XEREFI = 43.52 m.

The results of the convergence study are summarized in Table 4. Rows A–E show the convergence in space, rows F–J the convergence in time. Values in boldface (rows A and C) represent the parameters for convergence, and a further refinement gives variations below a few percent. Therefore, these values have been adopted for all inductive runs presented here. [4] Notice that the implied element size is of ∼0.25 cm in the refined region and of ∼7 cm in the rest of the domain.

For all resistive runs the following set of numerical parameters was used with MITHRANDIR: NELEMS = 1465, NELREF = 250, XBREFI = 40.0 m, XEREFI = 45.0 m, STPMIN = 1e−5 s, STPMAX = 5e−3 s, STPMAX2 = 5e−2 s. [5]

Concerning the computational performance, the MITHRANDIR runs presented in this work were performed on a Digital Alpha personal workstation 433 au operated by Unix, with 433 MHz clock and 256 MB RAM. A typical inductive run requires, with the above mentioned numerical parameters, about 15 min CPU time for the simulation of 1 min experimental time, and occupies about 18 MB real memory. However, notice that the very same run, on a Pentium laptop operated by Windows95, with 200 MHz clock and 64 MB RAM, takes about 2 h CPU time.

References

[1] Zanino R, Marinucci C. Heat slug propagation in QUELL. Part I: Experimental setup and 1-fluid GANDALF analysis, to appear in Cryogenics, 1999.
[2] Anghel A, et al., The quench experiment on long length (QUELL), Final report, 1997.
[3] Marinucci C, Bottura L, Vecsey G, Zanino R. The QUELL experiment as a validation tool for the numerical code Gandalf. Cryogenics 1998;38:467–77.

[4] The numerical parameters used by GANDALF for inductive runs are: NELEMS = 2000, NELREF = 500, XBREFI = 42.420 m, XEREFI = 43.620 m, STPMIN = 1e−5 s, STPMAX = 1e−3 s, STPMAX2 = 5e−2 s.

[5] The numerical parameters used by GANDALF for resistive runs are: NELEMS = 1465, NELREF = 250, XBREFI = 40.0m, XEREFI = 45.0m, STPMIN = 1e-5s, STPMAX = 1e-3s, STPMAX2 = 5e-2s.

[4] DePalo S, Marinucci C, Zanino R. Stability estimate for CICC with cooling channel using one-and two-fluid codes. Adv. Cryo. Engrg. 1998;43:333–9.
[5] Marinucci C, Savoldi L, Zanino R. Stability analysis of the ITER TF and CS conductors using the code Gandalf, to appear in IEEE Trans Appl Supercond, 1999.
[6] Zanino R, De Palo S, Bottura L. A two-fluid code for the thermohydraulic transient analysis of CICC superconducting magnets. J. Fus. Energy 1995;14:25–40.
[7] Zanino R, Bottura L, Marinucci C. A comparison between 1- and 2-fluid simulations of the QUELL conductor. IEEE Trans. Appl. Supercond. 1997;7:493–6.
[8] Martinez A, Turck B. Supercritical helium cooling of a cable in conduit conductor with an inner tube, 1993, CEA-DRFC-STIF Internal note P/EN/93.18 (29 pages).
[9] Duchateau, J.-L., Cable in conduit superconductors, 1998, in Handbook of applied superconductivity (Institute of Physics Publishing) chapter B6, p. 267.
[10] Shaji A, Freidberg JP. in Ref. [2], pp. 128–130.
[11] Streeter VL. editor. Handbook of fluid dynamics. New York:McGraw-Hill, 1961:16–92–16–96.
[12] Zanino R, Bottura L, Marinucci C. Computer simulation of quench propagation in quell. Adv. Cryo. Eng. 1998;43:181–8.
[13] Zanino R, Savoldi L, Tessarin F, Bottura L. Effects of bundle/hole coupling parameters in the two-fluid thermal-hydraulic analysis of quench propagation in two-channel cable-in-conduit conductors, to appear in IEEE Trans Appl Supercond, 1999.
[14] Shimada M. private communication, 1996.
[15] Hamada K. et al., Thermal and hydraulic measurement in the ITER QUELL experiments. Adv Cryo Eng 1998;43:197–204.
[16] Zanino R, Bottura L, Savoldi L, Rosso C. Mithrandir+: a two-channel model for thermal-hydraulic analysis of cable-in-conduit super-conductors cooled with helium I or II. Cryogenics 1998;38:525–31.
[17] Salpietro E. ITER toroidal field model coil (TFMC) design and construction. Fus. Technol. 1998;34:797–801.
[18] Komarek P, Salpietro E. The test facility for the ITER TF model coil. Fus. Engrg. Des. 1998;41:213–21.
[19] Mitchell N. et al., ITER CS model coil project. ICEC16 Proceedings 1997;763–766.
[20] Tsuji H. et al., ITER Central Solenoid Model Coil Test Program. 1998, presented at the 17th IAEA Fusion Energy Conference.
[21] Savoldi L, Zanino R, Bottura L. Simulation of thermal-hydraulic transients in two-channel CICC with self-consistent boundary conditions, Paper COC-6 to be presented at the Cryogenic Engineering Conference, Montreal (Quebec) Canada, July 12–16 1999.